Available online at www.sciencedirect.com
SCIENCE DIRECT®
Wear 256 (2004) 867–878
WEAR
www.elsevier.com/locate/wear

Wear prediction of ceramics

S.M. Hsu*, Ming Shen

National Institute of Standards and Technology, Gaithersburg, MD 20899, USA

Received 2 July 2003; received in revised form 24 September 2003; accepted 3 November 2003

Abstract

Advanced ceramics are increasingly being used for wear applications. Wear prediction of ceramics has become an important subject in these arenas. Ceramic wear is a complex function of microstructure, grain size and shape, grain boundary toughness, and the operating conditions. Wear prediction, therefore, needs to address not only the amount of wear for a given range of operating conditions, it also needs to address the location of wear transitions, and the onset of different dominant wear mechanisms. This paper reviews the various wear models developed by the authors over the years to predict wear, wear transitions, and wear under different mechanisms for ceramics. Finally, we investigate the feasibility of modeling across a range of materials and operating condition using a concept of contact severity and material property normalization process. This results in a model capable of predicting wear of ceramics to ±1 order of magnitude using only the material property and operating parameters.

Keywords: Ceramics; Alumina; Modeling; Silicon carbide; Silicon nitride; Wear map; Wear mechanism; Wear transition; Zirconia

1. Introduction

The ability to predict wear of materials is a universal challenge crucial to successful application of new materials into different technologies, from nanometer scale to micrometer scale. As more and more new materials become available, design guideline of these new materials in a comprehensive manner to predict performance and life time take on additional urgency. However, wear prediction is mired in confusion and controversy and most literature models are developed specifically for an application under certain operating conditions and for a specific pair of materials, hence limited applicability to other situations and materials. The lack of utilization of these models for design purposes suggests a need to reexamine wear prediction methodology from a fundamental way. This paper presents a systematic analysis of wear prediction on advanced ceramics as an example to illustrate a viable wear prediction methodology.

Advanced ceramics possess a unique combination of light weight, hardness, and chemical inertness. Thus they are often used in wear resistant applications. Their inherently brittle nature, however, creates a concern for potential premature catastrophic failures. Recent field success of ceramics in engines (water pumps seals, cam roller lifters, and wear pads), industrial pumps, and seals have alleviated many of these concerns. The strength and fatigue resistance of these materials have also increased substantially over the last decade. Wear life prediction, therefore becomes more important in providing much needed design guidelines for further application of ceramics.

Wear is a complex system function. As such, wear of a material is dependent on contact geometry, surface roughness, microstructural features, grain sizes, fracture toughness, speed, load, temperature, duration, environment, and lubrication. Most of the wear models tend to fall into two categories: wear mechanism models for a specific system under a specific operating condition; and correlational models that use wear data over a range of conditions to establish the exponents of a power law formula. Very few attempts were made to model wear of several materials over a wide range of operating conditions. This paper first reviews the existing models and then addresses various models that may be applied successfully for a single material over specific operating ranges as illustrated by a wear map. Four types of ceramics will be used: alumina, silicon nitride, silicon carbide, and zirconia. We will address modeling efforts across the four materials and see how different models behave. Finally, we will attempt to see whether a single model can be used to predict wear of four materials across a wide range of operating conditions.

* Corresponding author.
E-mail address: stephen.hsu@nist.gov (S.M. Hsu).

0043-1648/$ – see front matter © 2003 Published by Elsevier B.V.
doi:10.1016/j.wear.2003.11.002

1.1. Ceramic wear mechanisms

Brittle solids such as ceramics wear by fracture. When the applied mechanical stresses exceed the fracture strength of the solid surface, fracture occurs. The fracture strength is a complex function of composition, grain boundary energy release rate, grain fracture energy release rate (the G ratio), and the presence of defects and residual stresses on the surface either from machining or sintering. Under mild contact conditions (defined generally as the mild wear regime) where the macroscopic contact stresses are below the fracture strength, the asperity (surface roughness) contact may exceed the fracture criteria and localized fracture takes place. This often results in grain boundary cracking and grain pull-outs. Subsurface cracks can take place at the grain boundary or through the grains depending on the relative G ratios (energy release rate in the grain boundary versus the energy release rate through the grain). Therefore, one of the key parameters for ceramic wear is surface roughness or third body dimensions in that they affect directly the mechanical stress intensity surfaces encountered during wear. In addition, differential thermal stresses from high speed sliding add to the stress intensity and needs taken into account. Based on these factors, we can derive equations to predict wear, wear transitions, and overall wear as a function of operating conditions.

2. Review of wear models

Ceramics typically possess high compressive strength and weak tensile strength, so in most instances, tensile stresses cause the onset of wear in a contact, especially in the mild wear regime. Tensile stresses from an asperity sliding against the counterface cause microfracture on the surface as well as subsurface grain boundary dislocations. When the contact pressure is sufficiently high to cause fracture, compressive stresses are more important in causing wear.

There are many wear studies and proposed wear models on ceramics in the literature. The purpose of this paper is not to provide a comprehensive list of studies but rather suggest a particular line of attack to describe ceramic wear so only selected papers are cited. Most proposed wear models are based on a specific materials pair under rather narrow operating conditions [1–10]. These models are useful in elucidating the operating wear mechanism occurred under the experimental conditions. As such, their ability to predict wear does not extend to a wide range of operating conditions nor across a range of materials. For this reason, application of ceramic materials is still based on actual component testing rather than prediction.

Evans first proposed a lateral crack model to predict ceramic machining rate, i.e. wear by machining process [1]. He developed an equation using the extension of lateral cracks to model removal of materials under high compressive stresses. Kato proposed the use of a contact severity index to classify the different wear modes under various contact severities to represent the propensity of brittle fracture by using applied stress intensity against the material's fracture toughness [2–4]. The severity index, S_c, was derived using the maximum Hertzian contact stresses as the dominating stress term [2] and an average surface roughness. The severity index was later modified to S_{CF} by including the contribution from friction, thus it represented a combined mode I and mode II stress intensity [3]. More recently, a further modified severity index, S_{cm}, was derived from taking the maximum tensile stress as the dominating stress term in the stress intensity modeling [4]. All the above severity indexes used the surface roughness to represent preexisting cracks. In this approach, the material's microstructure was not included in the models. The tensile crack model proposed in [5] presented yet another approach to predict wear of ceramics by using the fracture mechanics formalism. A concept based on energy balance was adopted to derive the wear equation. Microstructural parameter such as grain size was incorporated in the model.

Since ceramics are insulators, thermal diffusitivity is relatively low. Under high speed dry sliding conditions, localized thermal heating can be substantial. Thermal shock accelerated wear was observed and modeled by Sibley and Allen [6] in 1962. Ting and Winer proposed a thermomechanical model to include the friction induced thermal stresses in the calculations of total stress [9]. A dimensionless parameter, Gt, was proposed to indicate the degree of thermal heating from asperity flash heating under atmospheric conditions [8]. Kong and Ashby proposed the use of both the bulk and flash temperature for the description of ceramic wear [10]. The effect of asperity flash heating under lubricated conditions was considered in these models. These models also suggest that asperity heating can dominate the wear processes even though the real of area of contact is small.

Models described above are successful in explaining wear data and highlight the dominant wear mechanisms under different operating conditions. Lateral crack model assumes a severe contact stress under which the material's microstructure does not have dominant effect. In the development of the contact severity, rolling contact experiments were used. In formulating the contact severity index S_c, the use of the maximum Hertzian pressure to represent the dominating stress field therefore is reasonable. Under sliding condition, contributions from frictional traction to the estimate of stress intensity will need to be introduced, as in the S_{CF} and S_{cm}. But the fundamental assumption in this case is that no severe wear process is dominant. These hidden assumptions built into the various models need to be understood in order to apply these models.

In pure sliding experiments across a large range of severity, do these models apply? The wear maps of four ceramic materials, alumina, zirconia, silicon nitride, and silicon nitride, under dry sliding condition have been reported [11]. This wear data set represents a comprehensive wear data of four representative ceramics across a large range of operating conditions where there are distinct wear transitions,

thermal shock induced accelerated wear, and tribochemistry moderated wear. The availability of this data set presents a unique opportunity to test various models to examine their applicability. In the following sections, the wear experimental procedure and data will be briefly described, followed by the results of the modeling analysis.

3. Wear experiments

The details of the experiments have been described elsewhere [11]. The tests were conducted by using a four-ball wear apparatus modified to run on a ball-on-three-flats configuration under dry condition. The ball specimens were 12.5 mm in diameter and the flat specimens were circular disks with 6.35 mm in diameter and 1.59 mm in thickness. The surface roughness of the samples was closely controlled at ~0.02 μm. Wear tests were conducted using a step-loading procedure. Table 1 lists the ranges of the operating conditions, applied load and sliding speed used.

The material property data of the four ceramics are shown in Fig. 1. The alumina is a sintered α-alumina with an equiaxed grains about 5 μm diameter (range from 2 to 15 μm). The zirconia is a pressureless sintered 100% tetragonal zirconia doped with a mass fraction of 4.7% Yttria with a grain size about 1 μm in diameter. The silicon nitride is a hot isostatically pressed (HIP) mixture of α-Si_3N_4 and β-Si_3N_4. The α-phase is primarily in equiaxed grains of size ≈ 0.5 μm, while the β-phase forms elongated grains, up to 1 μm in diameter and 2–5 μm in length. The silicon carbide is a sintered and post-HIPped silicon carbide mixed with equiaxed grains and elongated grains. Elongated grains

Table 1
Ranges of operating conditions and material properties among the four ceramics

Parameters	Unit	Range
Load	N	2–340
Mean Hertzian pressure	GPa	0.34–2.87
Speed	m/s	0.0019–0.19
Hardness	GPa	13–31
Fracture toughness	MPa $m^{1/2}$	3.2–8.5
Young's modulus	GPa	220–430
Density	Mg/m^3	3.2–6.5
Thermal conductivity	W/m °C	1.8–110
Thermal diffusivity	10^{-6} m^2/s	0.74–36.33
Grain size[a]	μm	0.3–15
Mean grain size[a], d_{50}	μm	0.5–5
Large grain, d_{90}/d_{50}		1–3.3
Aspect ratio		1–5

[a] Measures of grain size, d_{50} and d_{90} for elongated grains are the diameter of the grain.

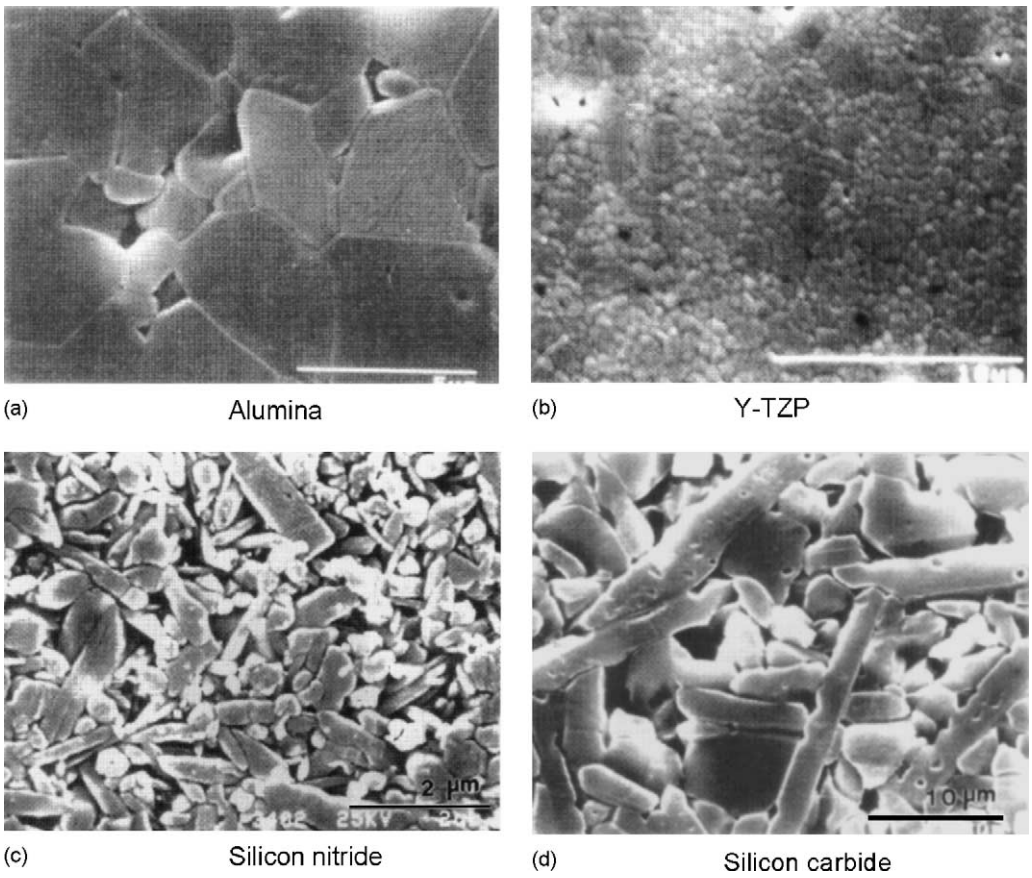

Fig. 1. Scanning electron micrographs (SEM) of etched flat samples of the four ceramics.

Table 2
Classification of the wear map data under dry sliding condition

Wear regime	Wear (mm^3)	Wear mechanism
Mild wear (stress intensity $< K_{1C}$)	10^{-7} to 10^{-4}	Asperity-scale failure mode: abrasion, intergranular cracks, subsurface damage/cracks, grain pullout, tribochemical
Severe wear (stress intensity $> K_{1C}$)	10^{-5} to 10^{-2}	Nominal scale failure mode: fracture mechanics, tensile cracks and edge effects, third-bodies (linked to grain pullout)
Ultra-severe wear (stress intensity $\gg K_{1C}$)	10^{-3} to 10^{1}	Nominal scale + few large debris, thermal shock (nominal scale)

are up to 2 μm in diameter and about 10–20 μm in length. Mainly α-phase SiC and a small amount of β-phase SiC are present.

3.1. Wear data classification

A large body of wear data was generated for the four ceramics and these data have been plotted as three-dimensional wear maps as a function of load and speed [11]. The wear volume data ranged from 10^{-7} to 10^{1} mm^3 among the four ceramics. In the three-dimensional wear maps, wear transitions can be observed visually and the wear transition boundaries are very distinct. Wear rate increases sharply across the transition zones. Based on these observations, we classify wear into mild, severe, and ultra-severe regimes and the associated wear levels shown in Table 2. This classification allows us to separate various dominant wear mechanisms in each regime. Abrasion and microfracture are the two dominant wear mechanisms in the mild wear regime, brittle fracture in the form of intergranular cracking is observed as the dominant wear mechanism in the severe wear regime. Gross fracture in the form of intragranular cracking and delaminational cracks (large flakes) are seen in the ultra-severe wear regime. The accelerated cracking can be attributed to thermal shock stresses under high speed high load conditions [13].

The observation and identification of the dominant wear mechanism for each regime provide an opportunity to conduct simple experiments (such as indentation, cracking, and one pass scratching tests) to identify the driving force behind each wear mechanism. Stress intensity in the contact has been identified as the critical parameter. In mild wear, the nominal contact produced stress intensity insufficient to cause macroscopic fracture. Wear occurred primarily at asperity tips either as abrasion or microfracture. This generates subsurface intergranular cracking [12] and leads to subsequent grain pullouts. In severe wear, the nominal contact pressure produces stress intensity that exceeds K_{1C} and causes microscopic fracture such as tensile cracks [13]. At the sharp edges of these cracks, stress intensity is high and wear occurs producing many wear particles [14]. These particles formed third-bodies in the contact and caused more localized fracture and grain pullouts resulting in larger wear particles being produced [15]. These large wear particles then serve to intensify the stress intensity inside the contact. Therefore, the high wear rate propagates. In the ultra-severe wear regime, intragranular fracture has been commonly observed. High loads and high speeds introduce additional differential thermal stresses due to the low thermal diffusitivity common to most ceramics.

4. Wear-mechanism-based models

Once the wear mechanism is understood, specific models can be formulated to describe the specific wear process. These models will be tested against the specific wear data in the specific regime(s) where the model is expected to work. The lateral crack model [1] and the tensile crack model [5] were tested against the wear data of silicon nitride in the severe wear regime:

- Lateral crack model (LCM):

$$\text{Wear vol} = C\frac{[E/H_V]^{4/5}}{K_{1C}^{1/2}H_V^{5/8}}N^{9/8}l \tag{1}$$

where C is the constant, N the load, l the distance slid, E the Young's modules, H_V the hardness and K_{1C} the fracture toughness.

- Tensile crack model:

$$\text{Wear vol} = C\frac{\sigma_{max}}{\sigma_D}\frac{Nl}{H_V(T)} \tag{2}$$

where σ_{MAX} is the maximum tensile stress, σ_D the critical damage stress, H_V the temperature-dependent hardness and T the temperature.

The presence of ultra-severe wear regime suggests that there is additional thermal stress to induce a higher rate of wear. Therefore, a thermal shock stress was modeled as follows [11]:

- Thermal shock stress:

$$\sigma_{thermal} = \frac{E\alpha}{1-\nu}\exp\left[\frac{-4}{\sqrt{\pi}}\left(\frac{T}{T^*}-5.3\right)\right] \tag{3}$$

where E is the Young's modules, α the linear expansion coefficient, ν the Poisson's ratio, T the flash temperature in [14], T^* the bulk temperature from nominal contact $= \mu NV/4aK$, N the load, V the speed, a the nominal Hertzian contact radius, K the thermal conductivity, and μ the friction coefficient.

In this model, an exponential functional dependence of the thermal stress as a function of the ratio of flash

temperatures to the surrounding surface temperatures was assumed. Subsequently, the maximum stress term in the TCM was assumed to be the sum of the mechanically induced tensile stress and the thermal shock stress, σ_{thermal}. The application of the thermal shock stress was limited only to the ultra-severe wear data.

- Wear transitions:

  Besides wear level predictions, the TCM was also tested for its applicability to predict the wear transitions. Due to its assumptions, it was best-suited for predicting the transition from mild to severe wear regimes. The onset of such wear transition was taken to be when the critical condition of $\sigma_{\text{MAX}}/\sigma_{\text{D}} = 1$ [5]. For the severe to ultra-severe wear transition, a thermal shock related model was needed. The critical velocity model (CVM) proposed in [6] was tested:

- Critical velocity model:

$$V_{\text{CR}} = \frac{4K^2}{(\mu\alpha E)^2 \pi\kappa z} \tag{4}$$

  where K the thermal conductivity, μ the coefficient of friction, α the coefficient of thermal expansion, E the Young's modules, κ the thermal diffusivity $= K/\rho c$, z the width of slider, ρ the density and c the specific heat.

  The onset of thermal shock damage was set to start when $V > V_{\text{CR}}$.

4.1. Identification of critical wear parameters in establishing new correlational models

Given a large data base of wear data, another approach to examine wear prediction across materials over a wide range of operating conditions is to explore correlational models against the critical material and operational parameters. For this purpose, let us examine the fundamental wear processes in an ideal contact model based on our understanding. Fig. 2 shows the schematic diagrams of various contact configurations under progressively more severe conditions. In the mild regime (a), wear can be treated as simple asperity-scale abrasion (microfracture does not produce wear immediately and grain pullouts are only intermittent). In this case, wear by each asperity contact can be approximated by the product of wear depth, contact width, and length of sliding within each "sliding cycle", as illustrated in Fig. 2(a). The "sliding cycle" can be described by the total distance slid l divided by the Hertzian contact width $2a$, i.e., $l/2a$. Given this set of assumptions, wear can be expressed as:

$$\text{Wear vol} \propto \left[\sum_i \left(\frac{P_{\text{m}}}{H_{\text{V}}} C_i d_i\right) d_i 2a\right] \frac{l}{2a} \tag{5}$$

where P_{m} the mean Hertzian pressure, H_{v} the hardness, C_i the dimensionless geometric factor and d_i the asperity contact width. The terms in the parenthesis represent the wear depth which is assumed to be proportional to the ratio of P_{m} and hardness and a fraction of the contact width d_i. The $2a$ term inside the bracket represents the upper bound of length l_i of such asperity-scale abrasive wear within a single cycle. Since the ratio of $P_{\text{m}}/H_{\text{v}}$ is constant throughout all the asperity contacts, the summation term will be proportional to the real area of contact which has been proposed to depend on [17,18] the following relationship:

$$A_{\text{real}} \propto \frac{N}{E'} f\,(\text{roughness parameters})$$

where N is the load and E' the composite Young's modulus. The roughness parameters included asperity radius [18], r.m.s. roughness [17,18], and/or autocorrelation length [17]. By substituting the real contact area into Eq. (5), the mild wear can be expressed by the following relationship:

$$\text{Wear vol} \propto \frac{P_{\text{m}}}{H_{\text{V}}} \frac{N}{E'} f\,(\text{roughness parameters}) \times l \tag{6}$$

Since the surface roughness of all specimens in this data set was controlled to be nearly the same, the roughness term, f, can be treated as a constant in this analysis. Hence, the mild wear was directly proportional to $P_{\text{m}} \times N \times l$, related to the operating parameters, and inversely proportional to material properties, H_{v} and E'.

In severe wear regime, because of the presence of cracks, edge effects from those cracks and third-body wear particles, the asperity contacts can have very different characteristics,

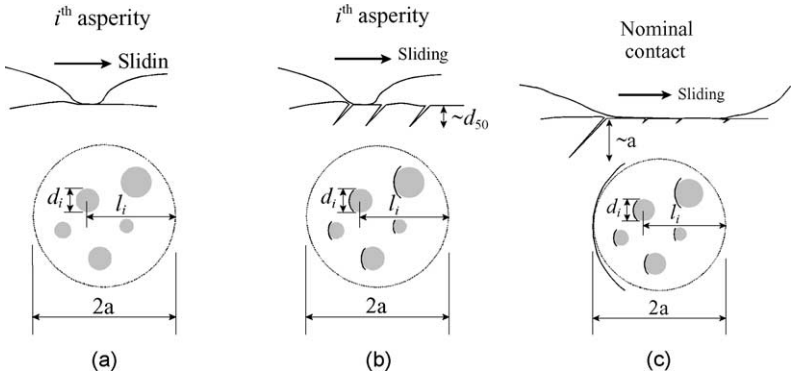

Fig. 2. Illustrations of the contacts for modeling wear in different wear regimes. (a) Asperity-scale abrasion in mild wear regime, (b) tensile cracks inside the nominal contact in severe wear regime, and (c) gross fracture in the nominal contact in ultra-severe wear regime.

as illustrated in Fig. 2(b). The total wear volume may be expressed as:

$$\text{Wear vol} \propto \left[\sum_i \frac{\sigma_{\max}(T^*/T_o)\sqrt{d_{50}}}{K_{1C}} \times b_i d_i \times d_i \times 2a\right] \frac{l}{2a} \tag{7}$$

where σ_{MAX} is the maximum tensile stress [4], T^* the interfacial temperature of the nominal contact [17], T_o the ambient temperature at 20 °C, K_{1C} the fracture toughness, d_{50} the mean grain size, b_i the geometric factor and d_i the contact width.

Here the wear depth is assumed to be proportional to the contact width d_i by using the ratio of a stress intensity from tensile stress divided by K_{1C} and another geometric factor b_i. The crack length in the measure of the stress intensity is assumed to be equivalent to the mean grain size d_{50}. Because of the potential thermal effects from frictional heating, the tensile stress is further modified by multiplying a temperature ratio of (T^*/T_o). The interfacial temperature T^* can be calculated by Archard's temperature equation [19]. In so doing, the nominal contact is treated as a single asperity and the interfacial temperature is applicable within a layer thickness of half of the Hertzian contact width, i.e., this temperature exists within a thickness of a. The multiple of the two d_i inside the bracket represents the real contact area, similar to the mild wear case. However, in the severe wear, a different interpretation may be needed to account for the edge effects due to cracking and third-body wear. This area is assumed to be proportional to the ratio of N/H_v [5]. Consequently, Eq. (7) could then be rewritten as follows:

$$\text{Wear vol} \propto \frac{\sigma_{\max}(T^*/T_o)\sqrt{d_{50}}}{K_{1C}} \frac{N}{H_V(T^*)} l \tag{8}$$

In Eq. (8) the hardness value is further set to include the temperature effects. Eq. (8) is similar to the tensile crack model proposed in [5] but with the added temperature effect. Also, the use of fracture toughness can eliminate the need for a special material property σ_D, the critical damage stress [5].

In ultra-severe wear regime, the thermal shock can be attributed to a temperature gradient between the heated spot and the surrounding low temperature region. Since the interfacial temperature exists in a layer with a thickness of half Hertzian width, the wear equation in Eq. (8) can be extended by substituting the d_{50} term with a, namely, the crack length that determines the stress intensity is equivalent to a, as illustrated in Fig. 2(c). This will give rise to an equation of the following form:

$$\text{Wear vol} \propto \frac{\sigma_{\max}(T^*/T_o)\sqrt{a}}{K_{1C}} \frac{N}{H_V(T^*)} l \tag{9}$$

The increased (T^*/T_o) ratio and crack length with a decrease in $H_v(T^*)$ should produce much higher wear level, as compared to the severe wear described in Eq. (8).

5. Correlational models examination against the data set

Armed with the existing models and the functional dependence of the fundamental wear processes, the wear data set is tested with different models. Many of the existing models cannot fit the large data set satisfactorily. Therefore, we embarked on an approach: the wear data set is plotted against a group of key parameters indicating the severity of the contact conditions. After the data are lined up according to the contact severity, then the materials will be normalized using material property data. In principle, such material normalization should eliminate the differences in material properties among different materials (provided that we know all of the important material properties related to wear). If this approach is successful, then a generalized wear equation for all materials over the entire operating range will line up according to some functional dependence.

5.1. Contact severity

The severity of the contact has been modeled by many [2–4,13,15]. As a group parameter, it is successful in the wear map concept illustrated by Adachi and Kato. However, we will show later that the contact severity index alone has limited applicability when it is used against a large data set. In the present approach, the severity parameter is defined as a group parameter directly reflecting the operating conditions. Let us reexamine each of the wear equations. In mild wear, Eq. (6) has two sets of parameters. The $P_m Nl$ term is related to the operating conditions. The $H_v E'$ is related to material properties. Similarly, the $\sigma_{MAX}(T^*/T_o)Nl$ term in Eq. (8) and the $\sigma_{MAX}\sqrt{a(T^*/T_o)Nl}$ term in Eq. (9) are related to the operating conditions and $\sqrt{d_{50}}/K_{1C}H_v(T^*)$ are related to the material property term in Eq. (8) and $K_{1C}H_v(T^*)$ in Eq. (9). So at this point, one can plot the wear data in each wear regime against the corresponding severity parameter and observe the data scatter among different materials. The degree of data scatter should reflect the validity of the choice of the operating parameters and the associated materials parameters. Therefore, a simple material normalization should be able to pack all the data of the same predominant wear mechanism into a single function with the severity parameter. This is the concept.

Clearly, the severity parameters determined from the three wear regimes are not identical. In order to test across the entire operating conditions (the three wear regimes) one needs to make some simplifications. Firstly, the common factor in all three wear regimes is Nl. The uncommon term in mild wear is P_m, in severe wear are $\sigma_{MAX}(T^*/T_o)$, and in ultra-severe wear are $\sigma_{MAX}\sqrt{a}(T^*/T_o)$. However, the P_m and σ_{MAX} are related via the coefficient of friction [13]. Moreover, the (T^*/T_o) is relatively close to unity in the mild wear regime for the four ceramics, except for Y-TZP. Therefore, the severity parameter can be generalized to a form of $\sigma_{MAX}(T^*/T_o)Nl$.

5.2. Materials normalization

Materials have been characterized historically by their material properties such as hardness, elastic modulus, toughness, thermal conductivity, thermal diffusivity, and the temperature influence on these properties. Yet at the same time, which of these parameters controls wear is not clear. Whether there are hidden parameters that are not obvious is also not clear (parameters such as grain boundary strength, population of defects, machining damage, grain geometry, residual stress, etc.). We know that brittle fracture behavior of ceramics is often influenced by the relative energy rate of the grain boundary governed by grain size, ratio of the grain boundary energy release rate versus the grain [20], and pre-existing defect population from sintering and machining. If the microstructure is a duplex structure, i.e., elongated grains intermixed with equiaxed grains, crack deflection by the elongated grains has to be taken into account, i.e., the aspect ratio of grain defined by grain length divided by grain diameter. Iteration between the severity index and material normalization parameters will test the validity of this concept and provide insight into an issue often eludes us in the past.

6. Results and discussion

6.1. Predictability of literature models

Fig. 3 shows the predictions of LCM and TCM for silicon nitride data. The lateral crack model contained a correlational constant C that needed to be determined. Other parameters were determined by using the experimental conditions and material properties. The constant C was determined by fitting the data point at a sliding speed of 0.0019 m/s and a normal load of 20 N. For the TCM, the critical damage stress, σ_D, for alumina was previously estimated from various sources [21], but the value of σ_D for Si_3N_4 was not available. We assumed that the damage stress was a constant and therefore could be incorporated into the fitting constant C to form a new constant C^*, i.e., $C^* = C/\sigma_D$. The friction coefficients were taken from experimental measurements. The temperature-dependent hardness, $H_V(T)$ was determined experimentally and the data were fitted into exponential functions to give $H_V(T) = 24\,e^{-0.00064T}$ for Si_3N_4. The temperature for each experimental wear datum was estimated by using the flash temperature model in [16]. Finally, the new constant C^* was determined by fitting the same data point used in testing LCM, i.e., at a speed of 0.0019 m/s and a normal load of 20 N. In the TCM, the flash temperature calculations required the estimation of the real contact area. A sensitivity analysis was performed by changing the radius of real contact area from 5 to 20 μm. The resulting flash temperatures were from 300 to 600 °C for Si_3N_4. Within these temperature ranges, the C values changed only about 5%. Thus, the model was fairly insensitive to the temperatures and real contact areas. Overall, good agreements with the experimental data were exhibited in the severe wear regime by both LCM and TCM. However, the models overestimated the wear level in the mild wear regime and underestimated in the ultra-severe wear regime.

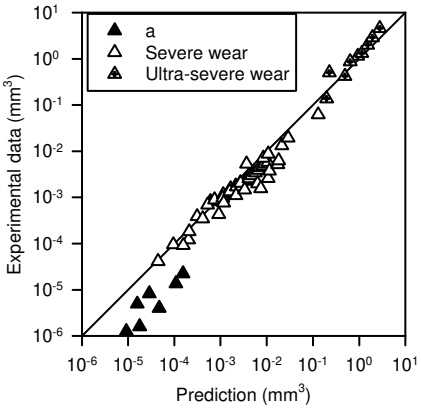

Fig. 4. Model predictions by TCM in severe and modified TCM in ultra-severe wear regimes of Si_3N_4.

Fig. 4 shows the prediction of TCM after the thermal shock stress was incorporated. Very good agreement

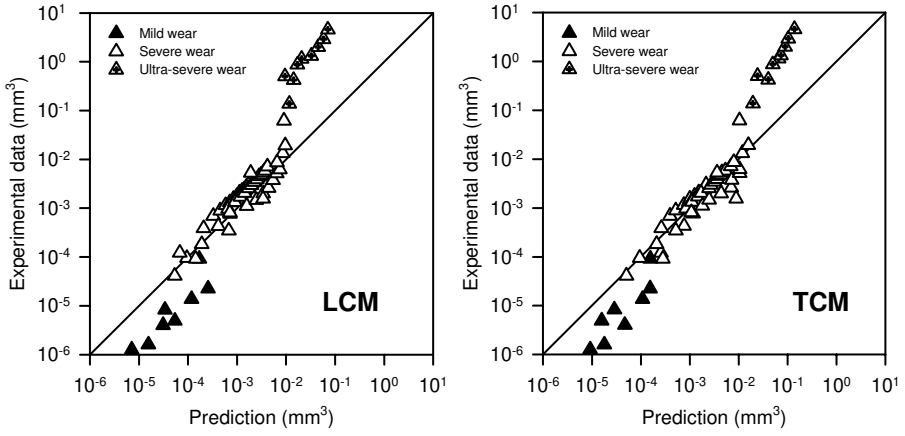

Fig. 3. Model predictions by LCM and TCM for Si_3N_4.

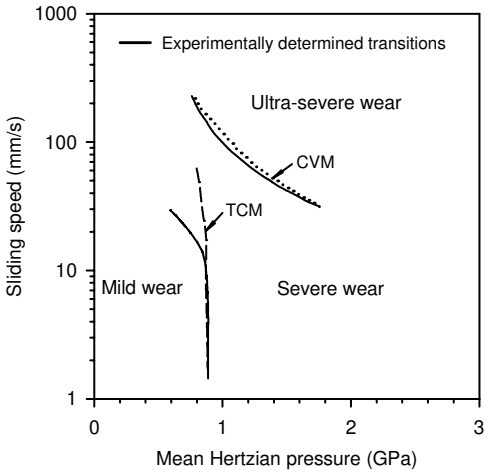

Fig. 5. Wear transition predictions by TCM and CVM for Si_3N_4.

between the model and data in the ultra-severe wear regime was obtained. This result confirmed that the additional thermal shock stress was responsible for the extremely high wear in the ultra-severe regime. Fig. 5 shows the predictions of wear transitions by using TCM and CVM. The TCM prediction had a slight deviation when the sliding speed was beyond 0.01 m/s. Meanwhile, the results from CVM matched well with experimentally determined wear transition, which was quite consistent with the wear level prediction by the modified TCM, i.e., additional stress by thermal shock could be accountable for the ultra-severe wear regime.

The results obtained by the existing brittle-fracture-based models were encouraging. Since wear of ceramics is dominated by brittle fracture, any fracture model with some reasonable fitting constants would describe the ceramic wear data somewhat satisfactorily. This may be the reason why the LCM and TCM perform similarly for the severe wear regime for silicon nitride. Speed was a factor, but only when the speed exceeded certain limits that it might induce thermal shock stresses that the fracture models began to underestimate. In the mild wear regime, the wear range was very large, from near-zero wear to 10^{-4}. This covers four orders of magnitude. Within this, tribochemical, plastic deformation, grooving, and single grain pullout are all dominant mechanisms. Fracture mechanics cannot account for these mechanisms, except maybe for grain pullouts. Therefore, it consistently overestimates the wear levels. The results of wear transition predictions also revealed some inadequacies in the existing models. The experimentally determined mild-to-severe wear transition could be predicted with some success by TCM. However, the model prediction overall was not quite satisfactory. This was probably due to the microstructural effects [22].

In the following section, historical severity indexes will be tested against the wear database, followed by the generalized severity parameter developed in the present study.

6.2. Historical severity indices

There were several versions of the so-called severity index proposed [2–4]. They are described below:

$$S_c = \frac{P_o\sqrt{R_{max}}}{K_{1C}} \tag{10}$$

where P_o is the maximum Hertzian pressure and R_{MAX} the maximum surface roughness. S_c was originally derived from modeling stress intensity factor by using the maximum Hertzian pressure and a crack length equivalent to the maximum surface roughness [2]. Subsequently, the severity index was modified by incorporating stresses introduced by friction and a slightly different form was derived [3] as shown below:

$$S_{CF} = \frac{P_o\sqrt{(1+\mu^2)R_{max}}}{K_{1C}} \tag{11}$$

where μ is the friction coefficient and the rest of the parameters were the same as in S_c. More recently, a new severity index derived from using the maximum tensile stress in estimation of threshold stress intensity, S_{cm}, was employed in describing the mild to severe wear of ceramic materials [4]. The maximum tensile stress was simplified in S_{cm}, as shown below:

$$S_{cm} = \frac{(1+10\mu)P_o\sqrt{R_{max}}}{K_{1C}} \tag{12}$$

where $(1+10\mu)P_o$ was the simplified tensile stress.

The maximum surface roughness, R_{MAX}, was the same in all specimens. Because it represented the equivalent crack length in the estimate of stress intensity, one could employ an alternative interpretation of this term by using the mean grain size.

Fig. 6 shows the applications of the various severity indexes to the wear map data from the four ceramics. The data of the mean grain size, d_{50}, of the four ceramics are listed in Table 3. The plots by using S_c and S_{CF} have quite similar features. Within each material, different wear levels could be present at the same severity index. Wear was mainly correlated by maximum Hertzian pressure in S_c, while friction coefficient had a slight contribution in S_{CF}. When all four materials were combined, they formed two groups. Alumina and SiC were in one group at higher severity. Silicon nitride and zirconia were in another group at lower severity. These were due to the combination of larger mean grain size and

Table 3
Microstructural parameters of the four ceramics, estimated from Fig. 1[a]

	Al_2O_3	Y-TZP	SiC	Si_3N_4
Mean grain size, d_{50} (μm)	5	1	3	0.5
Grain size ratio, d_{90}/d_{50}	3	2	2.6	2
Aspect ratio, A	1	1	5	4

[a] These are nominal dimensions based on the SEM micrographs with type B uncertainty of 50%.

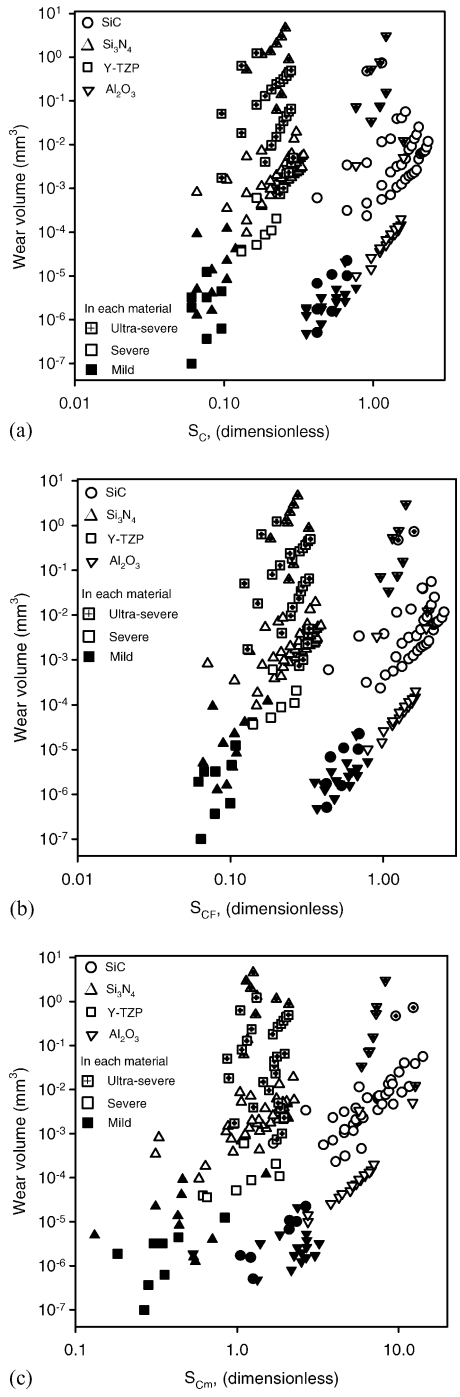

Fig. 6. Correlational results from using historical severity indexes: (a) S_c, (b) S_{CF}, and (c) S_{cm}. These indexes were defined in the text.

relatively lower fracture toughness in the alumina and SiC. On the other hand, Fig. 3(c) shows that the wear data mingled more by using S_{cm}. Because all these severity indexes already contained material properties, no material normalization could be applied. Therefore, one may conclude that they did not quite correlate with the current wear data.

Fig. 7 shows the application of a single parameter of mean Hertzian pressure to the database. Again, the results showed

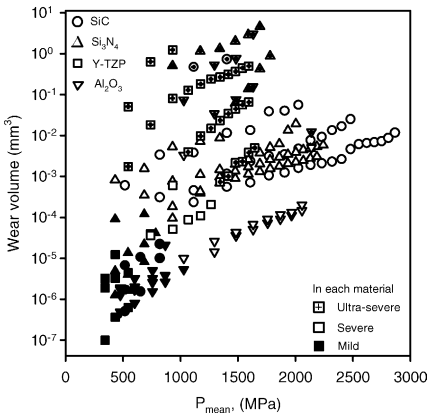

Fig. 7. Correlational results from using mean Hertzian contact pressure.

that it was inadequate to represent a unified severity parameter for this database.

6.3. Severity parameter from current work

Fig. 8(a) shows the wear data plotted by just using the $\sigma_{MAX}(T^*/T_o)$. This parameter had about three orders of magnitude range. As compared to the total range of wear

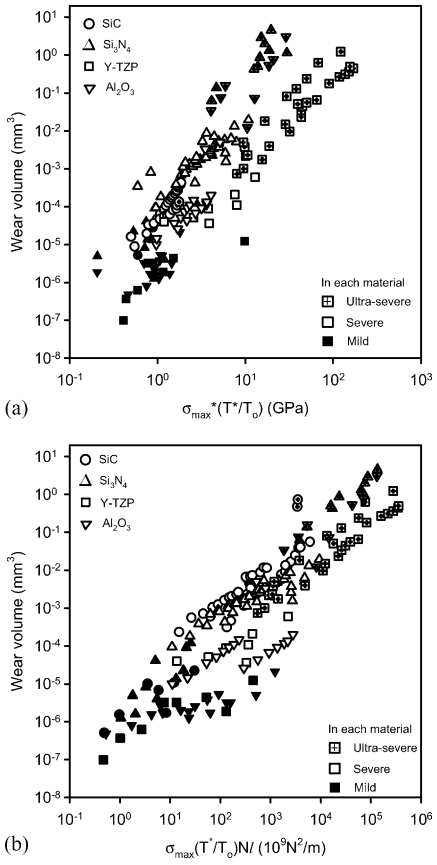

Fig. 8. Correlational results from using (a) maximum tensile stress multiplied by a temperature ratio of T^*/T_o to take into account the thermal effects and (b) a severity parameter derived from the current study.

volume of nine orders of magnitude, this parameter was extremely sensitive to wear. On the other hand, Fig. 8(b) shows the results from using severity parameter $\sigma_{MAX}(T^*/T_o)Nl$. This parameter had a range of seven orders of magnitude; this was much more comparable to the wear data range. Also the data in each wear regime appeared to form cluster, indicative of a rather reasonable selection of the severity parameter. Inclusion of $\sqrt{d_{50}}$ and $\sqrt{a}$ had also been tested. Only slight changes were obtained, so those plots were omitted from this presentation.

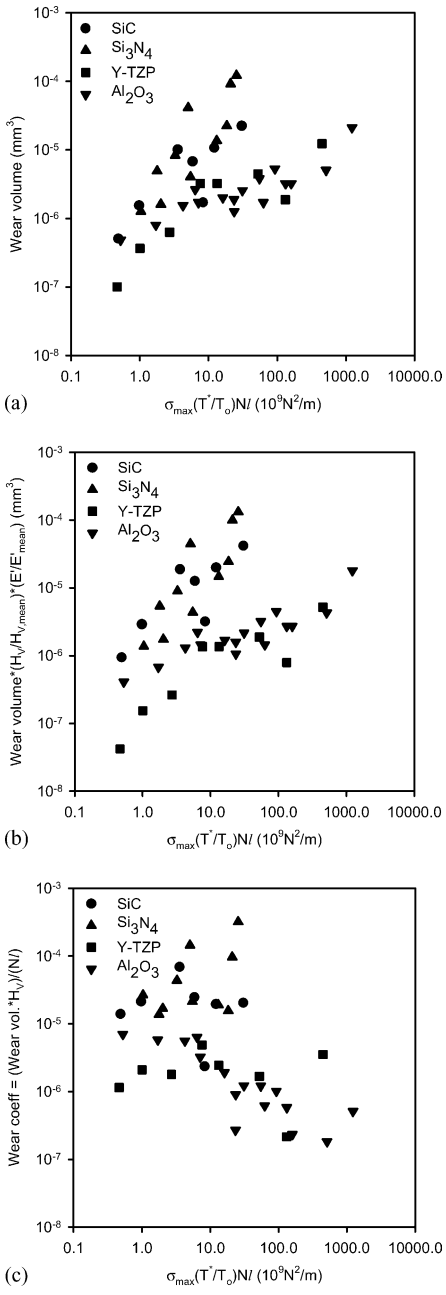

Fig. 9. Material normalization in the mild wear regime: (a) baseline (no normalization), (b) wear volume normalized by using the product of modified hardness and Young's modulus, and (c) normalization by using the wear coefficient.

6.4. Material normalization

There are different ways to normalize the wear results for the purpose of direct comparison. One way is to normalize all materials with respect to a particular material. Another is to determine the average value and then all materials will be normalized with respect to the average. The latter means was taken in the current work.

Fig. 9(a) shows the mild wear data separated from the whole group, and (b) shows the data being normalized against average H_V and average E'. The average H_V for the four materials was 21 ± 8 GPa and the average E' was 176 ± 44 GPa. Because wear in this regime, Eq. (6), was inversely proportional to these material properties, material normalization was carried out by multiplication of the wear volume by the ratios E'/E'_{mean} and $H_V/H_{V,mean}$. For example, the wear volume data of SiC were multiplied by 1.48 and 1.26, since its hardness and Young's modulus were both higher than the mean values. Fig. 9(b) displays that after material normalization, the Si-based ceramics were separated from the oxides. Because the functional dependence on the severity parameter was different between these two groups of data, different wear mechanism was controlling

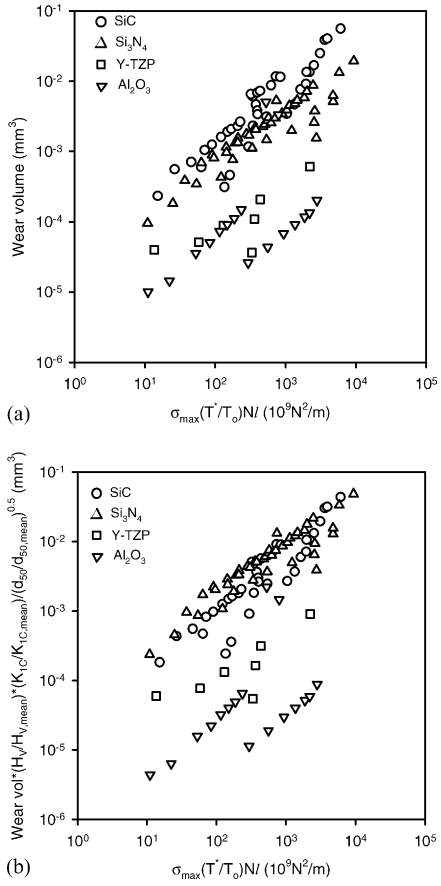

Fig. 10. Material normalization in the severe wear regime: (a) baseline (no normalization) and (b) wear volume normalized by the product of modified $H_V K_{1C}/\sqrt{d_{50}}$.

wear. One possible interpretation was that this could be caused by the tribochemical reactions, which were not included in the mechanism-based modeling. Fig. 9(c) presents a conventional material normalization scheme using the wear coefficient, defined as wear volume $\times H_V/(Nl)$. The results suggested that it was not applicable in this database.

Fig. 10 shows the material normalization carried out for data in the severe wear regime. According to Eq. (8), wear volume was inversely proportional to the product of $H_V(T^*)K_{1C}/\sqrt{d_{50}}$. The average fracture toughness for the four materials was $5.4 \pm 2.3\,\mathrm{MPa}\sqrt{m}$ and the average d_{50} was $2.4 \pm 2\,\mu\mathrm{m}$. Fig. 10(b) shows that the wear data among the two Si-based ceramics and Y-TZP appeared to be more packed. But the alumina data fell further away from the pack. There were two possible interpretations to such features. One was that the tribochemical reactions could have been extended into this regime among the fine wear particles. So the third-body wear has a significant effects on wear in alumina. The other could have been related to the data classification, i.e., the alumina data that fell away from the pack may need to be classified into mild wear regime. The material normalization used in [1] that correlated excellently with the grinding force data among different ceramics was also tested, i.e., $(K_{1C}^{0.625} \times H_v^{0.5})^{8/9}$. But only slight shifts were observed.

Fig. 11 shows the material normalization carried out for the ultra-severe wear data. The material normalization included the product of hardness and fracture toughness. The improvement from the material normalization appeared to be only slightly. Fig. 11(c) shows the use of wear coefficient to normalize the materials. The results did not confirm that it was applicable in this fast wearing regime, either.

The material normalization schemes in the above showed that different degrees of data shifts were obtained in the different wear regimes. Clearly, the process of selection of severity parameter and material normalization would be an iterative one, due to the simplification employed in the determination of severity parameters. Nevertheless, the process appeared to be in the correct direction. The overall data scatter after the material normalization was about ±1 order of magnitude.

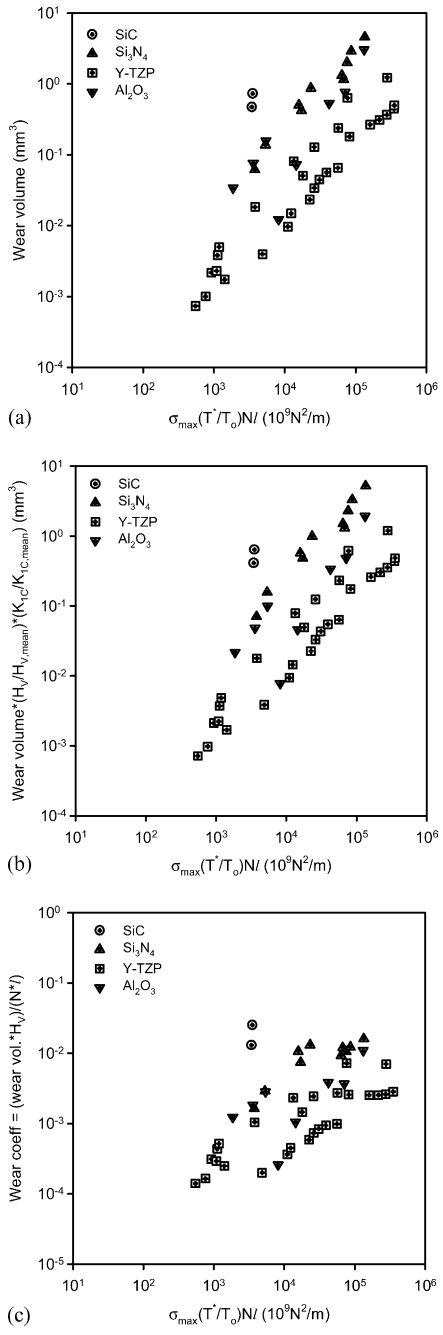

Fig. 11. Material normalization in the ultra-severe wear regime: (a) baseline (no normalization), (b) wear volume normalized by the product of modified hardness and fracture toughness, and (c) normalization by using wear coefficient.

7. Conclusions

The previously published wear maps presented a unique database where the experimental settings were self-consistent, and it contained wide variations in operating conditions and material properties. A new modeling methodology was developed in the current study and tested by using the wear map database. This methodology used severity parameter to separate the different wear regimes. The determination of the severity parameters was based on the understanding of the wear mechanisms derived from the wear maps. After the wear data of all four ceramics were separated by using the severity parameter, material normalization was carried out in the individual wear regimes. This was because the different predominant wear mechanisms in the individual regimes were associated with different material properties. The results showed that grouping of data among different ceramics was achieved through using the first sets of severity parameter and material normalization parameters. This was quite promising, in light of the huge variations present in the experimental conditions and materials. Further refinements through iterations would be necessary to reveal

or include other underlying factors that were not considered in the severity parameter as well as material normalization parameters. The contact severity concept proves to be more significant. The results from the material property normalization process suggest either there may be hidden material property parameters important to wear or there needs a new and novel normalization procedure.

References

[1] A.G. Evans, D.B. Marshall, Wear mechanisms in ceramics, in: Fundamentals of Friction and Wear of Materials, American Society of Metals, Metals Park, OH, 1980, p. 439.
[2] S.S. Kim, K. Kato, K. Hokkirigawa, H. Abe, Wear mechanism of ceramic materials in dry rolling friction, ASME J. Tribol. 108 (1986) 522.
[3] S.-S. Kim, S.-W. Kim, S.M. Hsu, A new parameter for assessment of ceramic wear, Wear 179 (1984) 69.
[4] K. Adachi, K. Kato, N. Chen, Wear map of ceramics, Wear 203–204 (1997) 291.
[5] Y. Wang, S.M. Hsu, Wear and wear transition modeling of ceramics, Wear 195 (1996) 35.
[6] L.B. Sibley, C.M. Allen, Friction and wear behavior of refractory materials at high sliding velocities and temperatures, Wear 5 (1962) 312.
[7] K.F. Dufrane, Sliding performance of ceramics for advanced heat engines, in: Proceedings of the Ceramic Engineering and Science, vol. 7, American Ceramic Society, 1986, p. 1052.
[8] J. Yang, W.O. Winer, A comparison between the thermomechanical wear theory and some experimental observations, ASME J. Tribol. 113 (1991) 262.
[9] B.Y. Ting, W.O. Winor, Friction-induced thermal influences in elastic contact between spherical asperities, ASME J. Tribol. 111 (1989) 315.
[10] H.S. Kong, M.F. Ashby, Wear mechanisms in brittle solids, Acta Metall. Mater. 40 (1992) 2907.
[11] S.M. Hsu, M.C. Shen, Ceramic wear maps, Wear 200 (1996) 154.
[12] S.J. Cho, H. Moon, B.J. Hockey, S.M. Hsu, Wear transition mechanism in alumina during sliding, Acta Metall. Mater. 40 (1) (1992) 185.
[13] S.M. Hsu, M.C. Shen, T.N. Ying, Y. Wang, S.W. Lee, Tribology of Si-based ceramics, Ceram. Trans. Am. Ceram. Soc. 42 (1994) 189.
[14] T.N. Ying, M.C. Shen, Y.S. Wang, S.M. Hsu, Tribology of Si-based ceramics—wear mechanisms, STLE Tribol. Trans. 40 (1997) 685.
[15] H.Y. Liu, S.M. Hsu, Modeling of micro-fracture-induced wear and wear transition of polycrystalline alumina under sliding, Wear 195 (1996) 169–177.
[16] H.S. Kong, M.F. Ashby, MRS Bull. 16 (1991) 41.
[17] S.C. Lee, H.S. Cheng, On the relation of load to average gap in the contact between surfaces with longitudinal roughness, STLE Tribol. Trans. 35 (1992) 523.
[18] J.A. Greenwood, J.B.P. Williamson, Contact of nominally flat surfaces, Proc. Roy. Soc. A 295 (1966) 300.
[19] J.F. Archard, The temperature of rubbing surfaces, Wear 2 (1958–1959) 438.
[20] M.Y. He, J.W. Hutchinson, Kinking of a crack out of an interface, J. Appl. Mech. 56 (1989) 271.
[21] S.-J. Cho, B.J. Hockey, B.R. Lawn, S.J. Bennison, J. Am. Ceram. Soc. 72 (1989) 1249.
[22] C. He, Microstructural effects on wear of ZrO_2–Al_2O_3 composites, Ph.D. Dissertation, University of Maryland, College Park, Maryland, 1995.